photonics

IMPACT FACTOR 1.9

CITESCORE 3.5

Communication

Optical Unidirectional Transport and Directional Blockade in Cold Atoms via Non-Hermitian Four-Wave Mixing

Xiao Liu, Maurizio Artoni, Giuseppe La Rocca and Jinhui Wu

MDPI

https://doi.org/10.3390/photonics12050521

photonics

MDPI

Communication

Optical Unidirectional Transport and Directional Blockade in Cold Atoms via Non-Hermitian Four-Wave Mixing

Xiao Liu [1], Maurizio Artoni [2,3], Giuseppe La Rocca [4] and Jinhui Wu [1,*]

[1] Center for Quantum Sciences and School of Physics, Northeast Normal University, Changchun 130024, China; liux866@nenu.edu.cn
[2] Department of Engineering and Information Technology, Brescia University, 25133 Brescia, Italy; maurizio.artoni@unibs.it
[3] European Laboratory for Nonlinear Spectroscopy, Istituto Nazionale di Ottica del CNR (CNR-INO), 50019 Sesto Fiorentino, Italy
[4] National Enterprise for Nanoscience and Nanotechnology, Scuola Normale Superiore, 56126 Pisa, Italy; giuseppe.larocca@sns.it
* Correspondence: jhwu@nenu.edu.cn

Abstract: We propose a scheme for realizing nonreciprocal optical scattering with non-Hermitian four-wave mixing (FWM) in a double-Λ system of cold atoms driven by coupling and dressing phase-mismatched standing-wave (SW) fields. Four scattering channels—direct transmission, cross transmission, direct reflection, and cross reflection—can be established for a probe and a signal field, some of which are nonreciprocal due to non-Hermitian spatial modulations when the two SW driving fields exhibit a $\pi/4$ phase shift. We find in particular that it is viable to attain single-color unidirectional transport, dual-color unidirectional transport, and single-color directional blockade with respect to a probe and a signal field incident upon this atomic sample from the same side, due to perfect destructive interference between direct and cross scattering channels. This work provides a new paradigm for studying non-Hermitian nonlinear optics and offers a theoretical foundation for designing all-optical atomic devices based on multi-channel nonreciprocal scattering.

Keywords: non-Hermitian four-wave mixing; multi-channel nonreciprocal scattering; unidirectional transport and directional blockade

Received: 7 April 2025
Revised: 9 May 2025
Accepted: 19 May 2025
Published: 21 May 2025

Citation: Liu, X.; Artoni, M.; La Rocca, G.; Wu, J. Optical Unidirectional Transport and Directional Blockade in Cold Atoms via Non-Hermitian Four-Wave Mixing. *Photonics* **2025**, *12*, 521. https://doi.org/10.3390/photonics12050521

1. Introduction

For a long time, four-wave mixing (FWM) has attracted the attention of numerous researchers due to its ability to manipulate information and transfer energy between optical fields of different frequencies and/or polarizations [1,2]. However, implementing FWM in conventional media faces challenges of weak nonlinear responses and significant resonant absorption, typically requiring high-intensity lasers or materials with special symmetries to enhance atom–light interactions. This limitation can be overcome by exploiting the effect of electromagnetically induced transparency (EIT) [3], which introduces a control field in multilevel atomic systems to suppress linear absorption at near-resonant frequencies via quantum destructive interference, thus enabling a coherent FWM of weak light signals via enhanced nonlinear susceptibility [4,5]. In view of this fact, EIT-based FWM in multilevel atomic systems has attracted broad interest recently, with most efforts focusing on exploring various laser coupling schemes [6–11] that enable important applications, including frequency conversion [11,12], squeezed light or biphoton generation [13,14], optical storage or quantum memory [15,16], and nonlinear optical amplification [17,18]. As a result, FWM

continues to be a highly relevant research topic, promising the development of advanced optical devices and quantum technologies, especially when working media like Rydberg atoms or driving schemes like non-Hermitian optics are incorporated [19,20].

On the other hand, optically tunable parity-time ($\mathcal{PT}$) symmetry and antisymmetry, as typical non-Hermitian effects, have been extensively studied in various EIT systems by making the control field and another external field exhibit out-of-phase spatially periodic modulations [21–31]. Leveraging $\mathcal{PT}$ symmetry and antisymmetry, a series of nontrivial optical phenomena can be achieved, including unidirectional reflectionless (URL) [25–27], asymmetric perfect absorption (APA) [27,28], and asymmetric diffraction [29–31]. This benefits indeed from the unusual feature $\chi_p(r) = \chi_p^*(-r)$ for $\mathcal{PT}$-symmetric systems while $\chi_p(r) = -\chi_p^*(-r)$ for $\mathcal{PT}$-antisymmetric systems with $\chi_p(r)$ being the complex susceptibility of a probe field at position r in an EIT medium. As far as we know, most non-Hermitian EIT studies focus on the linear regime because out-of-phase spatially periodic modulations of two external fields have already introduced abundant nontrivial optical phenomena along with theoretical and experimental complexities. Undoubtedly, if extended to the nonlinear regime, non-Hermitian EIT studies will significantly enhance the likelihood of realizing a broader spectrum of nontrivial optical phenomena, facilitating the development of advanced optical devices with multiple nonreciprocal scattering channels.

In this work, we consider a four-level double-Λ scheme of cold ^{87}Rb atoms driven by two strong fields (coupling or dressing) and two weak fields (probe or signal) to facilitate desired non-Hermitian FWM processes. We find that it is viable to realize a non-Hermitian atomic device exhibiting four scattering channels with respect to the probe and signal fields—direct and cross transmission as well as direct and cross reflection—when the coupling and dressing fields are set in the phase-mismatched standing-wave (SW) pattern. It is of more interest that one or two of the four output fields—forward and backward probes as well as forward and backward signals—may be quenched when both probe and signal input fields come from one side of this atomic sample. Such nonreciprocal scattering behaviors can be classified into 'single-color unidirectional transport', 'dual-color unidirectional transport', and 'single-color directional blockade', all of which arise from perfect destructive interference between relevant cross and direct scattering channels. Beyond expanding the scope of non-Hermitian optics into the nonlinear regime, our findings provide a theoretical blueprint for multi-channel scattering devices with all-optical tunability.

2. Model and Equations

We start by considering a four-level atomic system in the double-Λ configuration as shown in Figure 1a, where a probe field and a signal field of frequencies (amplitudes) ω_p and ω_s (E_p and E_s) drive, respectively, transitions $|1\rangle \leftrightarrow |3\rangle$ and $|1\rangle \leftrightarrow |4\rangle$, while a coupling field and a dressing field of frequencies (amplitudes) ω_c and ω_d (E_c and E_d) drive, respectively, transitions $|2\rangle \leftrightarrow |3\rangle$ and $|2\rangle \leftrightarrow |4\rangle$. These coherent light fields exhibit detunings (Rabi frequencies) $\Delta_p = \omega_p - \omega_{31}$, $\Delta_s = \omega_s - \omega_{41}$, $\Delta_c = \omega_c - \omega_{32}$, and $\Delta_d = \omega_d - \omega_{42}$ ($\Omega_p = E_p d_{13}/2\hbar$, $\Omega_s = E_s d_{14}/2\hbar$, $\Omega_c = E_c d_{23}/2\hbar$, and $\Omega_d = E_d d_{24}/2\hbar$) with ω_{ij} (d_{ij}) being resonant frequencies (dipole moments) on relevant atomic transitions. To avoid drive wrong transitions, each light field can be chosen with an appropriate polarization when the frequency difference between levels $|1\rangle$ and $|2\rangle$ is large enough, as detailed at the beginning of the next section. Two distinct FWM pathways are enabled in this system, governed by the energy conservation condition of $\Delta_p - \Delta_c + \Delta_d - \Delta_s = 0$. One follows the transition sequence $|1\rangle \to |3\rangle \to |2\rangle \to |4\rangle \to |1\rangle$, starting by absorbing ω_p photons and ending at emitting ω_s photons. The other proceeds via $|1\rangle \to |4\rangle \to |2\rangle \to |3\rangle \to |1\rangle$, starting by absorbing ω_s photons and ending at emitting ω_p photons. Significantly, in addition to inevitably existent direct transmission channels (referring to ω_p

or ω_s photons transmitting directly without frequency conversion), the two FWM pathways introduce cross transmission channels (referring to ω_p photons being converted into ω_s photons and then transmitted, or vice versa), which are inherently absent in traditional linear EIT systems where the probe and signal fields propagate independently.

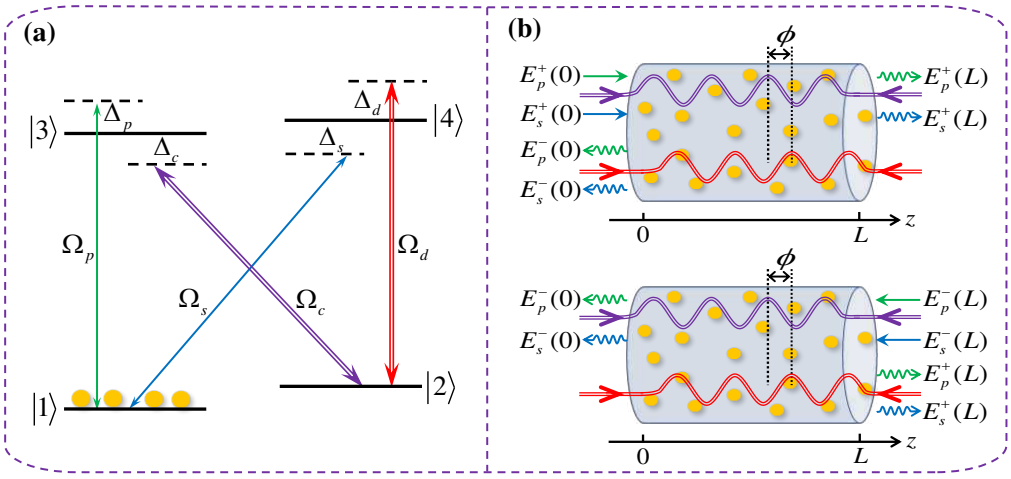

Figure 1. (**a**) The diagram of a four-level atomic system driven by a probe field and a signal weak field as well as coupling and dressing strong fields on relevant transitions to form a double-Λ configuration. The coupling, dressing, probe, and signal fields exhibit Rabi frequencies (detunings) Ω_c, Ω_d, Ω_p, and Ω_s (Δ_c, Δ_d, Δ_p, and Δ_s), respectively, while implementing a nonlinear FWM transition starting from and ending at the only populated ground level $|1\rangle$. (**b**) The schematic of two coherent FWM processes where a probe field and a signal field $\{E_p^+(0), E_s^+(0)\}$ input from the left side (upper panel) or $\{E_p^-(L), E_s^-(L)\}$ input from the right side (lower panel) are scattered by a sample of cold atoms in the double-Λ configuration, into two probe $\{E_p^+(L), E_p^-(0)\}$ and two signal $\{E_s^+(L), E_s^-(0)\}$ output fields. The coupling and dressing fields, each formed by two retroreflected light beams traveling along the $\pm z$ directions, are in the mismatched SW pattern with a phase shift ϕ.

We further assume that the coupling and dressing fields are in the SW pattern with

$$\begin{aligned} \Omega_c(z) &= 2G_c \cos(k_c z), \\ \Omega_d(z) &= 2G_d \cos(k_d z + \phi), \end{aligned} \tag{1}$$

where $k_c = 2\pi \cos\theta_c / \lambda_c$ and $k_d = 2\pi \cos\theta_d / \lambda_d$ represent the wavenumbers, while ϕ refers to a phase shift. In fact, both $\Omega_c(z)$ and $\Omega_d(z)$ are formed by two retroreflected light beams, which propagate along the $\pm z$ directions with the $\pm k_c$ and $\pm k_d$ wavenumbers, so that the probe and signal fields experience Bragg reflection and FWM in four different ways. Therefore, the two SW driving fields open up direct reflection channels (referring to ω_p or ω_s photons reflecting directly without frequency conversion), which cannot be achieved by traveling wave (TW) driving fields. Notably, we may take $k = k_c = k_d$, which is crucial for ensuring a common Bragg condition for both probe and signal fields so that their reflections can be simultaneously enhanced. Although λ_c and λ_d are slightly different, $k = k_c = k_d$ can be achieved through experimentation by carefully adjusting the small angles θ_c and θ_d of the SW coupling and dressing fields with respect to the z direction. Last but not least, the interplay between coherent FWM and Bragg reflection can give rise to a class of extra nontrivial scattering channels, namely cross reflection channels (referring to ω_p photons being converted into ω_s photons and then reflected, or vice versa).

Under both electric-dipole and rotating-wave approximations, with the above considerations, we can write down the Hamiltonian in the interaction picture as follows:

$$\begin{aligned} H_I = \; & -\hbar[\delta_2|2\rangle\langle 2| + \Delta_p|3\rangle\langle 3| + \delta_3|4\rangle\langle 4|] - \hbar[\Omega_p|3\rangle\langle 1| \\ & +\Omega_s|4\rangle\langle 1| + \Omega_c(z)|3\rangle\langle 2| + \Omega_d(z)|4\rangle\langle 2| + h.c.], \end{aligned} \tag{2}$$

where $\delta_2 = \Delta_p - \Delta_c$ and $\delta_3 = \Delta_p - \Delta_c + \Delta_d$ are two-photon and three-photon detunings, respectively. To account for population decay and coherence dephasing, respectively, with rates Γ_{ij} and γ_{ij}, we introduce the Lindblad superoperator $\mathcal{L}(\rho)$, which, together with H_I, can be employed to derive a set of dynamical equations governing the 16 density matrix elements ρ_{ij} associated with the double-Λ configuration in Figure 1(a). In the limit of weak probe and signal fields ($|\Omega_{p,s}| \ll G_{c,d}$) of interest, to the first-order of Ω_p and Ω_s, it is appropriate to set $\rho_{11}^{\langle 1\rangle} \simeq 1$ and $\rho_{22}^{\langle 1\rangle} \simeq \rho_{33}^{\langle 1\rangle} \simeq \rho_{44}^{\langle 1\rangle} \simeq \rho_{43}^{\langle 1\rangle} \simeq \rho_{42}^{\langle 1\rangle} \simeq \rho_{32}^{\langle 1\rangle} \simeq 0$ so that these dynamical equations of density matrix elements reduce to

$$\begin{aligned} \partial_t\rho_{21}^{\langle 1\rangle} &= -(\gamma_{21} - i\delta_2)\rho_{21}^{\langle 1\rangle} + i\Omega_c^*\rho_{31}^{\langle 1\rangle} + i\Omega_d^*\rho_{41}^{\langle 1\rangle}, \\ \partial_t\rho_{31}^{\langle 1\rangle} &= -(\gamma_{31} - i\Delta_p)\rho_{31}^{\langle 1\rangle} + i\Omega_c\rho_{21}^{\langle 1\rangle} + i\Omega_p, \\ \partial_t\rho_{41}^{\langle 1\rangle} &= -(\gamma_{41} - i\delta_3)\rho_{41}^{\langle 1\rangle} + i\Omega_d\rho_{21}^{\langle 1\rangle} + i\Omega_s. \end{aligned} \tag{3}$$

Setting $\partial_t\rho_{ij}^{\langle 1\rangle} = 0$ in the above equations, it is easy to cast the first-order steady-state solutions for the probe and signal coherences into a matrix form:

$$\begin{pmatrix} \rho_{31}^{\langle 1\rangle}(z) \\ \\ \rho_{41}^{\langle 1\rangle}(z) \end{pmatrix} = \frac{1}{\mathcal{D}(z)} \begin{pmatrix} \mathcal{A}(z) & \mathcal{B}(z) \\ \\ \mathcal{B}(z) & \mathcal{C}(z) \end{pmatrix} \begin{pmatrix} \Omega_p \\ \\ \Omega_s \end{pmatrix} \equiv \begin{pmatrix} A(z) & B(z) \\ \\ B(z) & C(z) \end{pmatrix} \begin{pmatrix} \Omega_p \\ \\ \Omega_s \end{pmatrix} \tag{4}$$

with $\mathcal{A}(z) = i[g_{21}g_{41} + \Omega_d^2(z)]$ and $\mathcal{C}(z) = i[g_{21}g_{31} + \Omega_c^2(z)]$ for the two diagonal elements while $\mathcal{B}(z) = -i\Omega_c(z)\Omega_d(z)$ for the common off-diagonal element and $\mathcal{D}(z) = g_{21}g_{31}g_{41} + g_{31}\Omega_d^2(z) + g_{41}\Omega_c^2(z)$ for the common denominator. We have also defined the complex dephasing rates $g_{21} = \gamma_{21} - i\delta_2$, $g_{31} = \gamma_{31} - i\Delta_p$, and $g_{41} = \gamma_{41} - i\delta_3$ for the spin (ρ_{21}), probe (ρ_{31}), and signal (ρ_{41}) coherences, respectively, with γ_{21} usually negligible because it is typically at least three-order of magnitude smaller than $\gamma_{31} \simeq \gamma_{41}$.

The diagonal (direct) terms $A(z)$ and $C(z)$ are the only ones that would survive in the absence of dressing and coupling fields, while the off-diagonal (crossed) terms $B(z)$ would vanish. Nonlinear wave-mixing effects mediated by these crossed terms play a key role in the scattering processes represented by Equation (4). It is worth noting that the signal affects the spatial distribution of the probe's coherence (polarization) in much the same way as the probe affects the spatial distribution of the signal's coherence. Such a symmetrical mutual influence—at least under the first-order approximation of Ω_p and Ω_s—is explicitly represented by two identical anti-diagonal matrix elements in Equation (4). When the dressing field vanishes, $\rho_{31}^{\langle 1\rangle}(z)$ in Equation (4) reduces to $ig_{21}\Omega_p/[g_{21}g_{31} + \Omega_c^2(z)]$, viz., the familiar coherence expression of a three-level *linear* EIT system. Similarly, we have $\rho_{41}^{\langle 1\rangle}(z) = ig_{21}\Omega_s/[g_{21}g_{41} + \Omega_d^2(z)]$ when there is no coupling field. In such linear EIT systems, significant advances have been made in achieving optically tunable $\mathcal{PT}$ symmetry or antisymmetry by exploiting the out-of-phase spatial modulation techniques [21–31]. Prompted by these advances, we now leverage the spatially mismatched SW coupling and dressing fields in the nonlinear FWM system shown in Figure 1a to attain a *non-Hermitian* optical response. This can be performed by shifting $\Omega_c(z)$ and $\Omega_d(z)$ by $\phi = \pi/4$, which clearly provides control capabilities beyond those of traditional linear systems.

Then, we build on a recent work [32] where only a probe *or* a signal enters the atomic sample to further address a new scenario where scattering involves instead of *both* probe and signal impinging simultaneously. A sketch of the scattering region ($z = 0 \leftrightarrow L$) is shown in Figure 1b, where the incident probe and signal pair—depicted as straight arrows—can enter from either left or right, while the four scattering channels—represented by wavy arrows—denote the outgoing waves after scattering. For the left incident case, viz., $E^{+}_{p,s}(0) \neq 0$ and $E^{-}_{p,s}(L) = 0$, the scattered fields comprise the *transmitted* pair $\{E^{+}_{p}(L), E^{+}_{s}(L)\}$, arising from the interference between direct and cross transmission channels, and the *reflected* pair $\{E^{-}_{p}(0), E^{-}_{s}(0)\}$ that arise instead from the interference between direct and cross reflection channels (see the upper panel). Conversely, for the right incident case, viz., $E^{-}_{p,s}(L) \neq 0$ and $E^{+}_{p,s}(0) = 0$, our non-Hermitian FWM scattering entails the transmitted pair $\{E^{-}_{p}(0), E^{-}_{s}(0)\}$ and the reflected pair $\{E^{+}_{p}(L), E^{+}_{s}(L)\}$ (see the lower panel). The two scattered pairs $\{E^{+}_{p}(L), E^{+}_{s}(L)\}$ and $\{E^{-}_{p}(0), E^{-}_{s}(0)\}$ are characterized by the following synthetic transmission and reflection coefficients (incidence from the left):

$$\begin{aligned}
t^{+}_{p}(L) &= E^{+}_{p}(L)/E^{+}_{in}(0) = \left[t^{++}_{pp}E^{+}_{p}(0) + t^{++}_{sp}E^{+}_{s}(0)\right]/E^{+}_{in}(0),\\
t^{+}_{s}(L) &= E^{+}_{s}(L)/E^{+}_{in}(0) = \left[t^{++}_{ps}E^{+}_{p}(0) + t^{++}_{ss}E^{+}_{s}(0)\right]/E^{+}_{in}(0),\\
r^{-}_{p}(0) &= E^{-}_{p}(0)/E^{+}_{in}(0) = \left[r^{+-}_{pp}E^{+}_{p}(0) + r^{+-}_{sp}E^{+}_{s}(0)\right]/E^{+}_{in}(0),\\
r^{-}_{s}(0) &= E^{-}_{s}(0)/E^{+}_{in}(0) = \left[r^{+-}_{ps}E^{+}_{p}(0) + r^{+-}_{ss}E^{+}_{s}(0)\right]/E^{+}_{in}(0),
\end{aligned} \tag{5}$$

with $E^{+}_{in}(0) = \sqrt{|E^{+}_{p}(0)|^2 + |E^{+}_{s}(0)|^2}$, or else (incident from the right)

$$\begin{aligned}
r^{+}_{p}(L) &= E^{+}_{p}(L)/E^{-}_{in}(L) = \left[r^{-+}_{pp}E^{-}_{p}(L) + r^{-+}_{sp}E^{-}_{s}(L)\right]/E^{-}_{in}(L)\\
r^{+}_{s}(L) &= E^{+}_{s}(L)/E^{-}_{in}(L) = \left[r^{-+}_{ps}E^{-}_{p}(L) + r^{-+}_{ss}E^{-}_{s}(L)\right]/E^{-}_{in}(L),\\
t^{-}_{p}(0) &= E^{-}_{p}(0)/E^{-}_{in}(L) = \left[t^{--}_{pp}E^{-}_{p}(L) + t^{--}_{sp}E^{-}_{s}(L)\right]/E^{-}_{in}(L),\\
t^{-}_{s}(0) &= E^{-}_{s}(0)/E^{-}_{in}(L) = \left[t^{--}_{ps}E^{-}_{p}(L) + t^{--}_{ss}E^{-}_{s}(L)\right]/E^{-}_{in}(L),
\end{aligned} \tag{6}$$

with $E^{-}_{in}(L) = \sqrt{|E^{-}_{p}(L)|^2 + |E^{-}_{s}(L)|^2}$. Here, t^{++}_{pp} and t^{++}_{ps} (r^{+-}_{pp} and r^{+-}_{ps}) represent the transmission (reflection) amplitudes for a left-input probe field, quantifying the direct and cross transmission (reflection) channels, respectively. The same definitions apply to t^{++}_{ss} and t^{++}_{sp} (r^{+-}_{ss} and r^{+-}_{sp}), yet for a left-input signal field. Symmetrically, when the probe and signal fields are input from the right side, analogous transmission and reflection amplitudes can be defined by swapping the two input directions with '$+ \leftrightarrow -$'.

All 16 transmission and reflection amplitudes inside the square brackets of Equations (5) and (6) can be computed by solving the steady-state Maxwell equations under the slowly varying envelope approximation with the consideration that both probe and signal fields contain forward $E^{+}_{p,s}(z)$ and backward $E^{-}_{p,s}(z)$ components. The polarization functions required to solve these Maxwell equations are $P_{31}(z) = Nd_{13}\rho^{\langle 1\rangle}_{31}(z) = Nd_{13}[A(z)\Omega_p + B(z)\Omega_s]$ and $P_{41}(z) = Nd_{14}\rho^{\langle 1\rangle}_{41}(z) = Nd_{14}[C(z)\Omega_s + B(z)\Omega_p]$ with N being the atomic density. They are here computed through the Fourier expansions of their space-dependent components according to $\mathrm{Y}(z) = \mathrm{Y}_0 + \mathrm{Y}_{1+}e^{i2kz} + \mathrm{Y}_{1-}e^{-i2kz} + \ldots$, where $\mathrm{Y} \in \{A, B, C\}$ and the zeroth-order Y_0 and the first-order $\mathrm{Y}_{1\pm}$ components are given by

$$\mathrm{Y}_0 = \frac{1}{a}\int_0^a \mathrm{Y}(z)dz \quad \text{and} \quad \mathrm{Y}_{1\pm} = \frac{1}{a}\int_0^a \mathrm{Y}(z)e^{\pm i2kz}dz \tag{7}$$

with $a = \pi/k$ being the common period of SW coupling and dressing fields. The coupled equations for the four-mode (probe and signal) electric fields $\{E_p^+(z), E_p^-(z), E_s^+(z), E_s^-(z)\}$ involved in the non-Hermitian FWM scattering process can be numerically solved under the condition of perfect phase matching ($\Delta k = k_p - k_c + k_d - k_s = 0$):

$$\frac{\partial}{\partial z}\begin{pmatrix} E_p^+ \\ E_p^- \\ E_s^+ \\ E_s^- \end{pmatrix} = \begin{pmatrix} \eta_p A_0 & \eta_p A_{1-} & \eta_p B_0 & \eta_p B_{1-} \\ -\eta_p A_{1+} & -\eta_p A_0 & -\eta_p B_{1+} & -\eta_p B_0 \\ \eta_s B_0 & \eta_s B_{1-} & \eta_s C_0 & \eta_s C_{1-} \\ -\eta_s B_{1+} & -\eta_s B_0 & -\eta_s C_{1+} & -\eta_s C_0 \end{pmatrix}\begin{pmatrix} E_p^+ \\ E_p^- \\ E_s^+ \\ E_s^- \end{pmatrix} = \hat{X}\begin{pmatrix} E_p^+ \\ E_p^- \\ E_s^+ \\ E_s^- \end{pmatrix}, \quad (8)$$

with $\eta_p = i\omega_p N d_{13}^2/4\hbar\epsilon_0 c$ and $\eta_s = i\omega_s N d_{14}^2/4\hbar\epsilon_0 c$. Here, we do not include a nonzero Δk because its main effect is to reduce the nonlinear conversion efficiency, as shown in [2,33], considering TW driving fields in an FWM process. A formal integration of this equation as detailed in Ref. [32] yields a 4×4 transfer matrix $\hat{M} = \hat{X}L$ that relates the electric fields $\{E_p^+(z), E_p^-(z), E_s^+(z), E_s^-(z)\}$ at two boundaries $z = 0$ and $z = L$. By applying single-input field boundary conditions adopted here (*i*) $E_p^+(0) = E_0$ and $E_s^+(0) = E_p^-(L) = E_s^-(L) = 0$; (*ii*) $E_s^+(0) = E_0$ and $E_p^+(0) = E_p^-(L) = E_s^-(L) = 0$; (*iii*) $E_p^-(L) = E_0$ and $E_p^+(0) = E_s^+(0) = E_s^-(L) = 0$; (*iv*) $E_s^-(L) = E_0$ and $E_p^+(0) = E_s^+(0) = E_p^-(L) = 0$, we could obtain with the help of the transfer-matrix elements M_{ij} the 16 complex amplitudes $\{r_{lm}^{\pm\mp}, t_{lm}^{\pm\pm}\}$ with $l, m = \{s, p\}$ [32] inside the square brackets of Equations (5) and (6) and, in turn, the 8 synthetic reflection and transmission coefficients $\{r_l^{\pm}, t_l^{\pm}\}$ with $l = \{s, p\}$.

3. Results and Discussion

In this section, our goal is to explore a few nonreciprocal scattering phenomena based on coherent FWM attained with out-of-phase periodic coupling and dressing fields, in the specific case where a probe field and a signal input field impinge upon the atomic sample from either the left or right side. We choose the D1 line of ^{87}Rb atoms as an example by taking $|1\rangle \equiv |5^2S_{1/2}, F = 1, m = 0\rangle$, $|2\rangle \equiv |5^2S_{1/2}, F = 2, m = 0\rangle$, $|3\rangle \equiv |5^2P_{1/2}, F = 1, m = 1\rangle$, and $|4\rangle \equiv |5^2P_{1/2}, F = 2, m = -1\rangle$ for the double-Λ system in Figure 1a. This then yields a frequency difference of 816 MHz between levels $|3\rangle$ and $|4\rangle$, while 6.83 GHz between levels $|1\rangle$ and $|2\rangle$ [34], with the probe and coupling fields being in the σ^+ polarization, and the signal and dressing fields being in the σ^- polarization. In this regard, we can make each optical field drive a desired transition, yet with negligible influences on all other transitions, either due to excessively large detunings or improper polarizations. Moreover, we have dephasing rates $\gamma_{21} = 2\pi \times 1$ kHz and $\gamma_{31,41} = 2\pi \times 3$ MHz, transition wavelengths $\lambda_{p,s,c,d} \simeq 795$ nm, and dipole moments $d_{14,24} = \sqrt{3}d_{13,23} = 1.268 \times 10^{-29}$ C·m [34].

To validate the non-Hermitian properties induced by out-of-phase periodic coupling and dressing fields, we plot in Figure 2 the moduli of all transmission and reflection amplitudes against the probe detuning Δ_p for symmetric driving fields of $G_c = G_d$ and $\Delta_c = \Delta_d$. We also take $\phi = \pi/4$ as a representative case because it corresponds to the most pronounced non-Hermitian spatial modulation maximizing the nonreciprocal scattering effects. As predicted in the last section, by combining nonlinear frequency conversion with Bragg reflection, we observe not only the omnipresent direct transmission amplitudes $|t_{pp,ss}^{\pm\pm}|$ but also the nonzero cross transmission amplitudes $|t_{ps,sp}^{\pm\pm}|$, direct reflection amplitudes $|r_{pp,ss}^{\pm\mp}|$, and cross reflection amplitudes $|r_{ps,sp}^{\pm\mp}|$. A notably interesting fact is that nonreciprocal behaviors occur for both cross transmissions and direct reflections with $|t_{ps,sp}^{++}| \neq |t_{ps,sp}^{--}|$ and $|r_{pp,ss}^{+-}| \neq |r_{pp,ss}^{-+}|$ (compare the red solid and blue dashed lines), while the direct transmissions and cross reflections are reciprocal with $|t_{pp,ss}^{++}| = |t_{pp,ss}^{--}|$ and $|r_{ps,sp}^{+-}| = |r_{ps,sp}^{-+}|$ (see the black solid lines). Moreover, we have an invariance upon the simultaneous exchange of input frequencies and directions with $|t_{pp,ss}^{++}| = |t_{ss,pp}^{--}|$, $|t_{ps,sp}^{++}| = |t_{sp,ps}^{--}|$, $|r_{pp,ss}^{+-}| = |r_{ss,pp}^{-+}|$,

and $|r^{+-}_{ps,sp}| = |r^{-+}_{sp,ps}|$. However, by applying asymmetric driving parameters ($G_c \neq G_d$ or $\Delta_c \neq \Delta_d$), we can not only break this invariance but also violate the reciprocity of cross reflections, resulting in $|r^{+-}_{ps,sp}| \neq |r^{-+}_{ps,sp}|$. This will be further clarified in subsequent discussion on synthetic transmission and reflection coefficients.

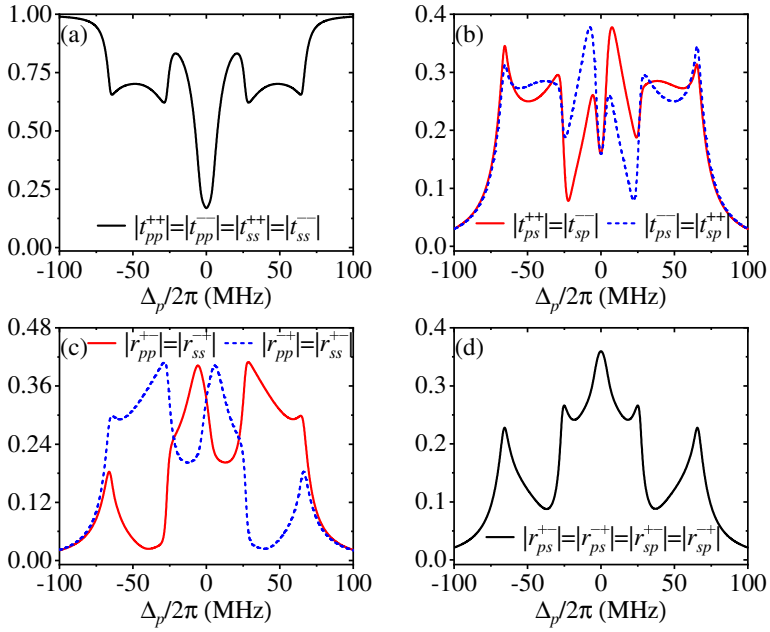

Figure 2. Moduli of direct (**a**) and cross (**b**) transmission amplitudes as well as direct (**c**) and cross (**d**) reflection amplitudes vs. probe detuning Δ_p. Other parameters are $G_c = G_d = 2\pi \times 70$ MHz, $\Delta_c = \Delta_d = 0$, $N = 1.0 \times 10^{12}$ cm^{-3}, $L = 1.2$ mm, and $\phi = \pi/4$.

Based on above nonreciprocal transmission and reflection amplitudes, four completely nonreciprocal output states with $t^+_p(L) \neq t^-_p(0)$, $t^+_s(L) \neq t^-_s(0)$, $r^-_p(0) \neq r^+_p(L)$, and $r^-_s(0) \neq r^+_s(L)$ can be obtained by comparing the case of $E^+_{p,s}(0) = E_{p,s}e^{i\phi_{p,s}}$ and $E^-_{p,s}(L) = 0$ with the case of $E^+_{p,s}(0) = 0$ and $E^-_{p,s}(L) = E_{p,s}e^{i\phi_{p,s}}$. This means that the probe and signal input fields coming from the left side and those coming from the right side should have identical amplitudes and phases when we make the comparison. We expect in particular that, when E_p and E_s as well as ϕ_p and ϕ_s satisfy specific conditions, perfect destructive interference may occur between relevant direct and cross scattering channels [see Equations (5) and (6)] to result in the quenching of one or two of the four (two probe and two signal) output fields. This then enables an interesting transition from nonreciprocal to unidirectional scattering behaviors, which will be validated through subsequent numerical results.

First, we try to prove that one of the four output fields can be quenched when the two input fields come from the right side but remains observable like others when the two input fields come from the left side. Such a single-color unidirectional transport, attained with symmetric driving parameters, is shown in Figure 3 by quenching the left probe output field $E^-_p(0)$ at a specific probe detuning for two right input fields $E^-_p(L)$ and $E^-_s(L)$ as an example. We find from the blue dashed lines that $|E^-_p(0) \propto t^-_p(0)|$ tends to be vanishing, while $|E^-_s(0) \propto t^-_s(0)|$, $|E^+_p(L) \propto r^+_p(L)|$, and $|E^+_s(L) \propto r^+_s(L)|$ are clearly nonzero, at $\Delta_p/2\pi = 14.2$ MHz [denoted by the vertical gray line in (a)] when the two right input fields exhibit an amplitude ratio $E_p/E_s = 0.4$ and a phase difference $\phi_p - \phi_s = 0.62\pi$. Meanwhile, we find from the red solid lines that all output fields are observable at the same probe detuning when the two input probe fields come from the left side with the same amplitude ratio and phase difference. Though not shown here, we note that it is also viable to obtain $|E^-_s(0)| \to 0$, $|E^+_p(L)| \to 0$, or $|E^+_s(L)| \to 0$ by modulating the two right input fields in

amplitude and phase, or achieve the same quenching results by modulating the two left input fields in amplitude and phase. Each of these single-color unidirectional transport behaviors is a result of perfect destructive interference between nonreciprocal reflection ($r_{pp}^{+-} \neq r_{pp}^{-+}$ or $r_{ss}^{+-} \neq r_{ss}^{-+}$) or transmission ($t_{sp}^{++} \neq t_{sp}^{--}$ or $t_{ps}^{++} \neq t_{ps}^{--}$) amplitudes, which is straightforward to understand by resorting to Equations (5) and (6).

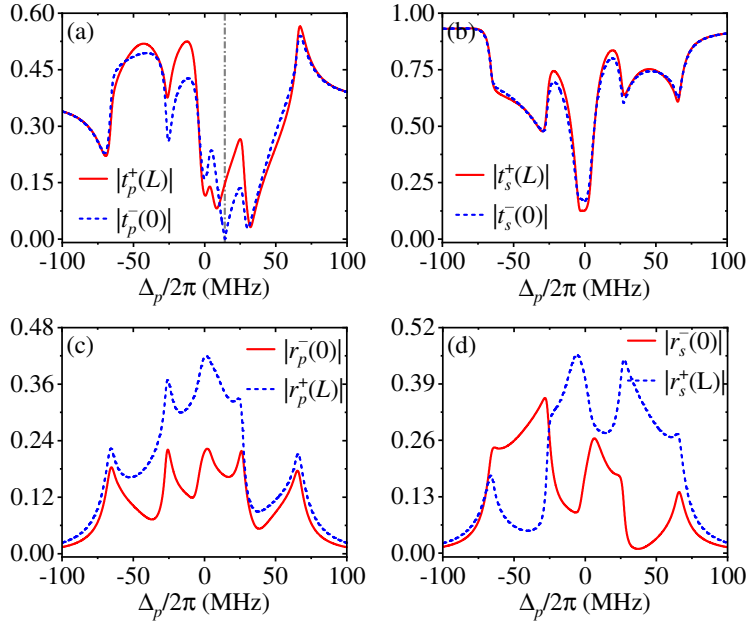

Figure 3. Moduli of synthetic transmission (**a**,**b**) and reflection (**c**,**d**) coefficients vs. probe detuning Δ_p attained with input field ratio $E_p^+(0)/E_s^+(0) = 0.4e^{i0.62\pi}$ (red solid) or $E_p^-(L)/E_s^-(L) = 0.4e^{i0.62\pi}$ (blue dashed). Other parameters are the same as in Figure 2.

Second, we try to prove that two output fields on the same side can be quenched when the two input fields come from the left side but remain observable when the two input fields come from the right side. Such a dual-color unidirectional transport, attained also with symmetric driving parameters, is shown in Figure 4 by quenching the right output fields $E_p^+(L)$ and $E_s^+(L)$ at a specific probe detuning for two left input fields $E_p^+(0)$ and $E_s^+(0)$ as an example. It is easy to find from the red solid lines that both $|E_p^+(L) \propto t_p^+(L)|$ and $|E_s^+(L) \propto t_s^+(L)|$ tend to be vanishing, while $|E_p^-(0) \propto r_p^-(0)|$ and $|E_s^-(0) \propto r_s^-(0)|$ are evidently nonzero, at $\Delta_p/2\pi \simeq -0.1$ MHz [denoted by the vertical gray lines in (a) and (b)] when the two left input fields exhibit an amplitude ratio $E_p/E_s = 1.0$ and a phase difference $\phi_p - \phi_s = 0.89\pi$. Meanwhile, we find from the blue dashed lines that all output fields are observable at the same probe detuning when the two input probe fields come from the right side with the same amplitude ratio and phase difference. Though not shown here, it is also viable to obtain $|E_p^-(0)| \to 0$ and $|E_s^-(0)| \to 0$ by modulating the two left input fields in amplitude and phase, or achieve the same nonreciprocal quenching results by modulating the two right input fields in amplitude and phase. Both types of dual-color unidirectional transport can also be attributed to a perfect destructive interference, which, however, involves either two pairs of nonreciprocal reflection ($r_{pp}^{+-} \neq r_{pp}^{-+}$ and $r_{ss}^{+-} \neq r_{ss}^{-+}$) or transmission ($t_{sp}^{++} \neq t_{sp}^{--}$ and $t_{ps}^{++} \neq t_{ps}^{--}$) amplitudes in Equations (5) and (6).

Finally, we try to prove that one of the four output fields can be quenched with the other three being always observable regardless of whether the two input fields come from the left side or the right side. Such a single-color directional blockade, attained with asymmetric driving parameters ($G_c \neq G_d$) instead, is shown in Figure 5 by quenching the left probe output field $E_p^-(0)$ at a specific probe detuning in both cases of two left input fields $E_{p,s}^+(0)$ and two right input fields $E_{p,s}^-(L)$ as an example. It is easy to find

from the blue dashed lines that $|E_p^-(0) \propto t_p^-(0)|$ tends to be vanishing, while $|E_s^-(0) \propto t_s^-(0)|$, $|E_p^+(L) \propto r_p^+(L)|$, and $|E_s^+(L) \propto r_s^+(L)|$ are clearly nonzero, at $\Delta_p/2\pi = 4.7$ MHz [denoted by the vertical gray line in (a)] for two right input fields with $E_p/E_s = 1.53$ and $\phi_p - \phi_s = 0.51\pi$. It is also evident from the red solid lines that $|E_p^-(0) \propto r_p^-(0)|$ tends to be vanishing, while $|E_s^-(0) \propto r_s^-(0)|$, $|E_p^+(L) \propto t_p^+(L)|$, and $|E_s^+(L) \propto t_s^+(L)|$ are clearly nonzero, at $\Delta_p/2\pi = 4.7$ MHz [denoted by the vertical gray line in (c)] for two left input fields with $E_p/E_s = 1.53$ and $\phi_p - \phi_s = 0.51\pi$. The single-color directional blockade featured by both $|t_p^-(0)| = 0$ and $|r_p^-(0)| = 0$ is also resulted from perfect destructive interference, which further involves nonreciprocal cross reflections ($r_{sp}^{+-} \neq r_{sp}^{-+}$) in addition to nonreciprocal direct reflections ($r_{pp}^{+-} \neq r_{pp}^{-+}$) and nonreciprocal cross transmissions ($t_{sp}^{++} \neq t_{sp}^{--}$) due to asymmetric driving parameters. Though not shown here, we have checked that it is also viable to obtain $|E_s^-(0)| \to 0$, $|E_p^+(L)| \to 0$, or $|E_s^+(L)| \to 0$ regardless of whether the two input fields with appropriate amplitude ratios and phase differences come from the left side or right side.

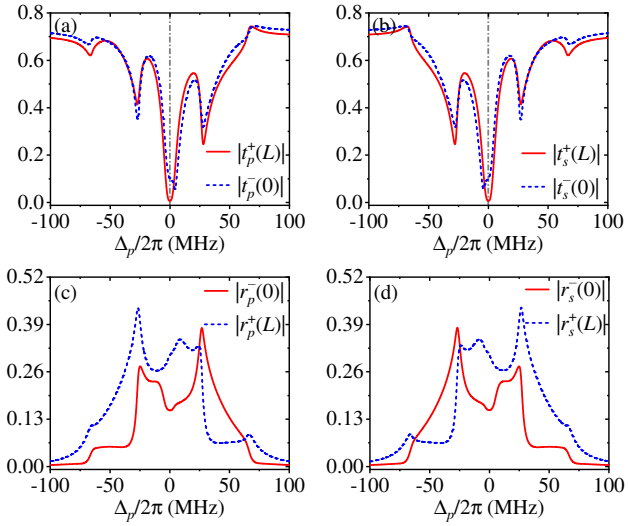

Figure 4. Moduli of synthetic transmission (**a**,**b**) and reflection (**c**,**d**) coefficients vs. probe detuning Δ_p attained with input field ratio $E_p^+(0)/E_s^+(0) = 1.0e^{i0.89\pi}$ (red solid) or $E_p^-(L)/E_s^-(L) = 1.0e^{i0.89\pi}$ (blue dashed). Other parameters are the same as in Figure 2.

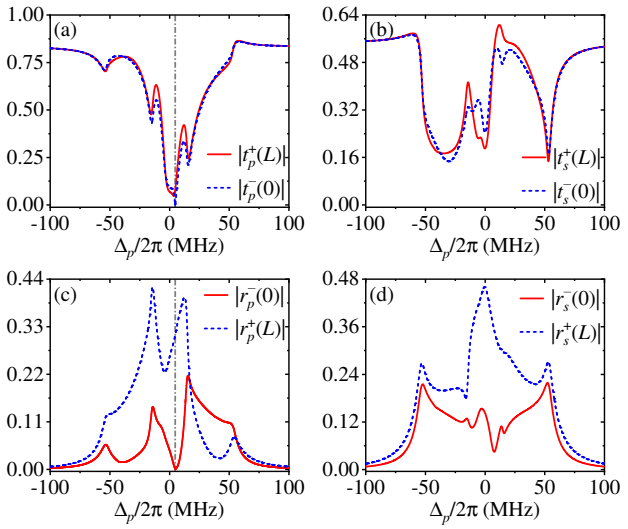

Figure 5. Moduli of synthetic transmission (**a**,**b**) and reflection (**c**,**d**) coefficients vs. probe detuning Δ_p attained with input field ratio $E_p^+(0)/E_s^+(0) = 1.53e^{i0.51\pi}$ (red solid) or $E_p^-(L)/E_s^-(L) = 1.53e^{i0.51\pi}$ (blue dashed). Other parameters are the same as in Figure 2 except $G_d = 2.22G_c = 2\pi \times 70$ MHz.

4. Conclusions

In summary, by combining the intrinsic nonlinearities of an FWM process occurring in multilevel systems with a phase-mismatched SW driving geometry to enhance Bragg reflection, we anticipate advanced control capabilities over nonreciprocal optical scattering beyond those of traditional linear systems. In our specific implementation within an atomic system, this combination enables the formation of four fundamental scattering channels: direct and cross transmission channels as well as direct and cross reflection channels. For a spatial phase shift $\phi = \pi/4$, this atomic system exhibits a non-Hermitian optical response, which enables the selective quenching of one or two of the four output fields by harnessing perfect destructive interference between direct and cross scattering channels, thus leading to single-color unidirectional transport, dual-color unidirectional transport, and single-color directional blockade. Our results point at not only a paradigm for exploring non-Hermitian nonlinear optical scattering but also to a framework for designing all-optically controlled multi-channel scattering devices, with potential extensions to non-atomic setups [35,36] and to higher-dimensional [30,31] non-Hermitian optical gratings.

Author Contributions: Conceptualization, X.L. and J.W.; methodology, X.L. and J.W.; software, X.L.; validation, X.L.; formal analysis, X.L., M.A., G.L.R. and J.W.; writing—original draft preparation, X.L.; writing—review and editing, M.A., G.L.R. and J.W.; visualization, X.L.; project administration, J.W. All authors have read and agreed to the published version of the manuscript.

Funding: This work is supported by the National Natural Science Foundation of China (No. 62375047), the Italian PNRR MUR (No. PE0000023-NQSTI), I-PHOQS (Photonics and Quantum Sciences, PdGP/GePro 2024-2026), and the Fund for International Activities of the University of Brescia.

Institutional Review Board Statement: Not applicable.

Informed Consent Statement: Not applicable.

Data Availability Statement: The raw data supporting the conclusions of this article will be made available by the authors on request.

Conflicts of Interest: The authors declare no conflicts of interest.

References

1. Asadpour, S.H.; Hamedi, H.R.; Paspalakis, E. Transfer of Orbital Angular Momentum of Light Using Autler-Townes Splitting. *Photonics* **2022**, *9*, 954. [CrossRef]
2. Meng, C.; Shui, T.; Yang, W.X. Coherent transfer of optical vortices via backward four-wave mixing in a double-Λ atomic system. *Phys. Rev. A* **2023**, *107*, 053712. [CrossRef]
3. Fleischhauer, M.; Imamoglu, A.; Marangos, J.P. Electromagnetically induced transparency: Optics in coherent media. *Rev. Mod. Phys.* **2005**, *77*, 633–673. [CrossRef]
4. Harris, S.E.; Field, J.E.; Imamoğlu, A. Nonlinear optical processes using electromagnetically induced transparency. *Phys. Rev. Lett.* **1990**, *64*, 1107–1110. [CrossRef]
5. Kang, H.; Hernandez, G.; Zhu, Y. Resonant four-wave mixing with slow light. *Phys. Rev. A* **2004**, *70*, 061804. [CrossRef]
6. Kumar, R.; Manchaiah, D.; Ahmad, M.; Easwaran, R.K. Effect of relaxation on the transfer of orbital angular momentum via four-wave mixing process in the four-level double lambda atomic system. *New J. Phys.* **2024**, *26*, 053045. [CrossRef]
7. Yang, B.; Xu, J.; Fan, J.; Zhou, H. Frequency characteristics of collimated blue light generated by four-wave mixing in cesium vapor. *Opt. Lett.* **2024**, *49*, 3846–3849. [CrossRef]
8. Wu, J.; Guo, M.; Zhou, H.; Liu, J.; Li, J.; Zhang, J. Experimental realization of efficient nondegenerate four-wave mixing in cesium atoms. *Opt. Express* **2022**, *30*, 12576–12585. [CrossRef]
9. Ullah, Z.; Wang, Z.; Gao, M.; Zhang, D.; Zhang, Y.; Gao, H.; Zhang, Y. Observation of the four wave mixing photonic band gap signal in electromagnetically induced grating. *Opt. Express* **2014**, *22*, 29544–29553. [CrossRef]
10. Du, S.; Oh, E.; Wen, J.; Rubin, M.H. Four-wave mixing in three-level systems: Interference and entanglement. *Phys. Rev. A* **2007**, *76*, 013803. [CrossRef]
11. Chiu, C.K.; Chen, Y.H.; Chen, Y.C.; Yu, I.A.; Chen, Y.C.; Chen, Y.F. Low-light-level four-wave mixing by quantum interference. *Phys. Rev. A* **2014**, *89*, 023839. [CrossRef]

12. Cheng, C.Y.; Liu, Z.Y.; Hu, P.S.; Wang, T.N.; Chien, C.Y.; Lin, J.K.; Juo, J.Y.; Shiu, J.S.; Yu, I.A.; Chen, Y.C.; Chen, Y.F. Efficient frequency conversion based on resonant four-wave mixing. *Opt. Lett.* **2021**, *46*, 681–684. [CrossRef] [PubMed]
13. Turnbull, M.T.; Petrov, P.G.; Embrey, C.S.; Marino, A.M.; Boyer, V. Role of the phase-matching condition in nondegenerate four-wave mixing in hot vapors for the generation of squeezed states of light. *Phys. Rev. A* **2013**, *88*, 033845. [CrossRef]
14. Shiu, J.S.; Lin, C.W.; Huang, Y.C.; Lin, M.J.; Huang, I.C.; Wu, T.H.; Kuan, P.C.; Chen, Y.F. Frequency-tunable biphoton generation via spontaneous four-wave mixing. *Phys. Rev. A* **2024**, *110*, 063723. [CrossRef]
15. Phillips, N.B.; Gorshkov, A.V.; Novikova, I. Light storage in an optically thick atomic ensemble under conditions of electromagnetically induced transparency and four-wave mixing. *Phys. Rev. A* **2011**, *83*, 063823. [CrossRef]
16. Wu, J.; Liu, Y.; Ding, D.S.; Zhou, Z.Y.; Shi, B.S.; Guo, G.C. Light storage based on four-wave mixing and electromagnetically induced transparency in cold atoms. *Phys. Rev. A* **2013**, *87*, 013845. [CrossRef]
17. Li, H.C.; Ge, G.Q.; Zubairy, M.S. Achieving nonlinear optical modulation via four-wave mixing in a four-level atomic system. *Phys. Rev. A* **2018**, *97*, 053826. [CrossRef]
18. Geng, Y.; Pei, X.; Li, G.; Lin, X.; Zhang, H.; Yan, D.; Yang, H. Spatial susceptibility modulation and controlled unidirectional reflection amplification via four-wave mixing. *Opt. Express* **2023**, *31*, 38228–38239. [CrossRef]
19. Zhao, H.M.; Zhang, X.J.; Artoni, M.; La Rocca, G.; Wu, J.H. Nonlocal Rydberg enhancement for four-wave-mixing biphoton generation. *Phys. Rev. A* **2024**, *109*, 043711. [CrossRef]
20. Jiang, Y.; Mei, Y.; Zuo, Y.; Zhai, Y.; Li, J.; Wen, J.; Du, S. Anti-parity-time symmetric optical four-wave-mixing in cold atoms. *Phys. Rev. Lett.* **2019**, *123*, 193604. [CrossRef]
21. Zhang, Z.; Zhang, Y.; Sheng, J.; Yang, L.; Miri, M.A.; Christodoulides, D.N.; He, B.; Zhang, Y.; Xiao, M. Observation of Parity-Time Symmetry in Optically Induced Atomic Lattices. *Phys. Rev. Lett.* **2016**, *117*, 123601. [CrossRef]
22. Yu, Q.; Yuan, J.; Liu, Z.; He, R.; Liang, S.; Zhang, Y.; Zhang, Z. Discrete dynamics of light in an anti-parity-time symmetric photonic lattice in atomic vapors. *Opt. Lett.* **2023**, *48*, 5735–5738. [CrossRef] [PubMed]
23. Li, H.J.; Dou, J.P.; Huang, G. $\mathcal{PT}$ symmetry via electromagnetically induced transparency. *Opt. Express* **2013**, *21*, 32053–32062. [CrossRef]
24. Sheng, J.; Miri, M.A.; Christodoulides, D.N.; Xiao, M. $\mathcal{PT}$-symmetric optical potentials in a coherent atomic medium. *Phys. Rev. A* **2013**, *88*, 041803(R). [CrossRef]
25. Chaung, Y.L.; Shamsi, A.; Abbas, M.; Ziauddin Coherent control of nonreciprocal reflections with spatial modulation coupling in parity-time symmetric atomic lattice. *Opt. Express* **2020**, *28*, 1701–1713. [CrossRef] [PubMed]
26. He, Y.; Wu, J.; Hu, Y.;Zhang, J.X.; Zhu, S.Y. Unidirectional reflectionless anti-parity-time-symmetric photonic lattices of thermal atoms. *Phys. Rev. A* **2022**, *105*, 043712. [CrossRef]
27. Liu, X.; Wu, J.H. Unidirectional and bidirectional photon transport blockade in driven atomic lattices of parity-time antisymmetry. *New J. Phys.* **2024**, *26*, 013048. [CrossRef]
28. Wu, J.H.; Artoni, M.; La Rocca, G. Perfect absorption and no reflection in disordered photonic crystals. *Phys. Rev. A* **2017**, *95*, 053862. [CrossRef]
29. Hang, C.; Li, W.; Huang, G. Nonlinear light diffraction by electromagnetically induced gratings with $\mathcal{PT}$ symmetry in a Rydberg atomic gas. *Phys. Rev. A* **2019**, *100*, 043807. [CrossRef]
30. Shui, T.; Yang, W.X.; Liu, S.; Li, L.; Zhu, Z. Asymmetric diffraction by atomic gratings with optical $\mathcal{PT}$ symmetry in the Raman-Nath regime. *Phys. Rev. A* **2018**, *97*, 033819. [CrossRef]
31. Shui, T.; Yang, W.X.; Li, L.; Wang, X. Lop-sided Raman–Nath diffraction in $\mathcal{PT}$-antisymmetric atomic lattices. *Opt. Lett.* **2019**, *44*, 2089–2092. [CrossRef] [PubMed]
32. Liu, X.; Artoni, M.; La Rocca, G.; Wu, J.H. Non-Hermitian optical scattering in cold atoms via four-wave mixing. *arXiv* **2025**, arXiv:2504.03127. [CrossRef]
33. Shui, T.; Yang, W.X.; Cheng, M.T.; Lee, R.K. Optical nonreciprocity and nonreciprocal photonic devices with directional four-wave mixing effect. *Opt. Express* **2022**, *30*, 6284–6299. [CrossRef] [PubMed]
34. Steck, D.A. Rubidium 87 D Line Data. Available online: http://steck.us/alkalidata (accessed on 8 June 2024).
35. Heinze, G.; Hubrich, C.; Halfmann, T. Stopped Light and Image Storage by Electromagnetically Induced Transparency up to the Regime of One Minute. *Phys. Rev. Lett.* **2013**, *111*, 033601. [CrossRef]
36. Chesi, S.; Artoni, M.; La Rocca, G.; Bassani, F.; Mysyrowicz, A. Polaritonic Stop-Band Transparency via Exciton-Biexciton Coupling in CuCl. *Phys. Rev. Lett.* **2003**, *91*, 057402. [CrossRef]